*Egypt. J. Chem.* **Vol. 65,** No. SI:13B pp. 941 - 948 (2022)

**Egyptian Journal of Chemistry**

**http://ejchem.journals.ekb.eg/**

# Synthesis and characterization of $Ho^{3+}$: $Yb^{3+}$ embedded silica–titania nanocomposites: structural and optical properties.

**Hanaa Shaier[1], Abeer Salah[2], Wafaa M. Mousa[1], Sawsan S. Hamed[1], Safaa K. El-Mahy[1], Inas K. Battisha3**

*1 Physics Department, Faculty of women for Arts, Science and Education, Ain Shams University, Cairo, Egypt,*
*2 Laser sciences and Interactions department, National Institute of Laser Enhanced Sciences (NILES), Cairo University, Egypt*
*3 Solid State Physics Department, Physics Research Institute, National Research Centre, Dokki, Giza 12622, Egypt, Affiliation ID: 60014618.*

**Abstract**

$Ho^{3+}$: $Yb^{3+}$ ions doped highly transparent $SiO_2$- $TiO_2$ nano-composite were successfully fabricated in the forms of monolith and thin films. the preparations were carried out via a modified sol-gel method at different annealing temperatures ranging from 500ºC up to 1000ºC for 3h. The structural and optical properties were determined by XRD, FESEM, 3D laser Raman and FTIR spectroscopy. The thickness of the thin film sample doped with 0.4 mol % of $Ho^{3+}$ ions and co-doped with 0.5mol % of $Yb^{3+}$ was measured 1.3 μm using the cross-section Field emission scanning electron microscopy (FESEM) technique. These results suggest that the $Ho^{3+}$: $Yb^{3+}$ silica-titania are promising candidates for photonic devices.

*Key Words*: Monolith, Thin film, Sol-Gel, Nano-composite ST, $Ho^{3+}$ and $Ho^{3+}$: $Yb^{3+}$ions and Optical properties.

## 1. Introduction

In recent years, rare-earth (RE) doped materials have attracted considerable attention owing to their potential for photonic applications in color displays, sensors, solar cells, detection of infrared radiation, and up-conversion (UC) lasers [1-3]. these materials are capable of efficiently converting infrared radiation into visible light. UC fluorescence emissions are obtained in different materials through doping ions, changing the ion doping concentration, or building complex structures. To date, $Er^{3+}$/$Yb^{3+}$, $Ho^{3+}$/$Yb^{3+}$, and $Tm^{3+}$/$Yb^{3+}$ emitter/absorber pairs have been widely employed as wave guide and upconverters [4,5].

Silica, titania, and their composite mixture represent a new class of materials that have attracted much attention from researchers [6-9]. These silica-titania (Si–Ti) mixed oxides have considerable interest due to their specific properties such as thermal stability, high porosity, and large surface area and are widely used as catalyst and catalyst supports [10-13], photocatalysts [14], thin-film coatings [15] and optic [16-17]. In fact, with respect to other technologies which are employed to develop photonic materials, sol-gel processing exhibits several advantages in terms of rare earth solubility, composition, design, tailoring of optical properties as well as fabrication of films, waveguides, and photonic crystals [18]. In particular, rare-earth-doped glasses, prepared by the sol-gel route, are used in a large number of optical applications, because of the multiple absorptions and emission bands available using the various rare-earth elements, and are becoming one of the cheapest and most versatile methods for the fabrication of integrated optics components [2, 19]. Glasses doped with rare earth ions are of great significance because these glasses have found many applications in devices such as solid-state lasers, upconverters, and optical fibers.

Characterization of such samples is mandatory in any research work. The characterization could be based on molecular spectroscopy like FTIR, Raman, Photoluminescence, or even molecular modeling **[20-30]**. If the elemental analysis is the aim of the characterization process hence several techniques could be utilized such as Atomic absorption, ICP, neutron activation, XRD…etc [31-32].

The main goal of the present work is to prepare the $Ho^{3+}$: $Yb^{3+}$ ions doped $SiO_2$- $TiO_2$ nano-composite via a modified sol-gel method at different annealing temperatures ranging from 500ºC up to 1000ºC for 3h.

The FTIR was utilized to identify the function groups, moreover to understand the crystal phases XRD was used. Raman spectra show that anatase and

*Corresponding author e-mail: szbasha5@yahoo.com.; (Inas K. Battisha).
Receive Date: 11 August 2022, Revise Date: 19 August 2022, Accept Date: 31 August 2022
DOI: 10.21608/EJCHEM.2022.155657.6723

rutile spectral features in the sample annealed up to 800ºC. The thickness of the thin film was measured using FESEM. To detect the high transparency of the prepared films annealed at 500ºC UV –Visible was used.

## 2. Experimental

### 2.1 Material

The chemical reagents used for $SiO_2$– $TiO_2$ (ST) co-doped with Rare Earth elements such as $Ho^{3+}$ ions and co-doped with $Ho^{3+}$ and $Yb^{3+}$ ions are listed in Table1. Tetraethyl orthosilicate (TEOS) $(C_2H_5O)_4Si$ as $SiO_2$ precursor, Titanium (IV) n-butoxide $Ti(OC_4H_9)_4$ as $TiO_2$ precursor, Holmium nitrate hydrate $Ho(NO_3)_3.H_2O$ as ($Ho^{3+}$ ions), Ytterbium nitrate pentahydrate $Yb(NO_3)_3.5H_2O$, ethanol ($CH_3CH_2OH$) solution, distilled water ($H_2O$), and HCl. Their compound, molecular weight, chemical form, symbols, and purity are shown in Table.1.

Table. 1.The compound, chemical formula, molecular weight and purity of the used materials.

| Compound | Chemical form | Molecular weight | Purity % | Company000000000000000 |
|---|---|---|---|---|
| Tetraethyorthosilicate (TEOS) | $(C_2H_5O)_4Si$ | 208.33 | 99 | Merck, Germany |
| Ethanol | $C_2H_5OH$ | 46.07 | 99.50 % | SiC, |
| Titanium(IV)n-butoxide | $Ti(C_4H_9O)_4$ | 340.35 | 98+ | Sigma–Aldrich, Germany |
| Acetyl acetone | $C_5H_8O_2$ | 100.12 | ≥98 | Fluka, Switzerland |
| Hydrochloric Acid | HCl | 36.46 | 34 | Adwic,El-Nasr Chemicals, |
| Holmium nitrate hydrate. | $Ho(NO_3)_3.H_2O$ | 350.95 | 99.9 | Sigma–Aldrich, Germany |
| Ytterbium nitrate pentahydrate | $Yb(NO_3)_3.5H_2O$ | 449.13 | 99.9 | Sigma–Aldrich, Germany |

### 2.2. Sample preparation

Nano-composites Silica-Titania in the monolith and thin film form containing (90 mol % $SiO_2$ –10 mol % $TiO_2$) referred to as (ST) were prepared using a modified sol-gel technique. First, the tetraethyl orthosilicate (TEOS) was dissolved in ethanol ($CH_3CH_2OH$) solution, then hydrolyzed under vigorous stirring after being dissolved in distilled water ($H_2O$) and the HCl was added to be used as a catalyst. In order to have solutions with a constant concentration of Si/Ti molar ratios: 90/10. The obtained solution was stirred for 1h at room temperature. The $Ho^{3+}$ ions were introduced in the process, by dissolving Ho $(NO_3)_3$-$H_2O$, in the obtained solution with molar ratios (0.4mol%) and activated with different concentrations of $Yb_2O_3$ as follows (0.5, 0.75, and 1mol % $Yb^{3+}$). These solutions stirred for another 30 min giving the solution (S1) solution. Titanium (IV) n-butoxide dissolved separately in acetyl acetone solution and stirred for 30 min solution then added to the obtained solution giving solutionS2. The final used mixture solution was homogeneous, transparent, and clear and no precipitates appeared. The resultant homogeneous solutions are divided into two parts monolith materials and thin film.

The resultant solutions of monolith materials were kept in closed glass vials and/or square plastic boxes during the gelation process which starts at the moment giving the hydrolyzed species in the mixture. All samples were aged for 21 days at 60ºC. Then the samples were heated at 500, 800, and 1000ºC for 3h, Muffle furnace type Carbolite CWF1200 was used for sample calcinations with a heating rate up 0.2ºC/ min down 0.4ºC/ min.

For thin film preparations; The prepared nanocomposite solutions were dropped and dispersed on glass substrates. The solutions then allowed spinning at 3500 revs. /Min for 30 seconds by using a homemade spin coater. At least two successive coatings were required to provide suitable effective film thickness. The film samples were dried and then heated at 500ºC for 3h, giving cracks free, homogeneous, clear, and transparent thin films useful for photonic applications.

The prepared samples are referred as; [ST0.4H0.5YM, ST0.4H0.75YM, and ST0.4H1YM] and [ST0.4H0.5YT, ST0.4H0.75YT, and ST0.4H1YT] for monolithic and thin film samples, respectively.

### 2.3. Characterization

#### 2.3.1.X-ray diffraction measurements (XRD)

XRD is the most essential tool used to characterize crystal structures. Evaluation of crystal structure is important for nano-scale materials since the material's properties may be affected on the nanometer scale. The XRD patterns and crystallinity of the prepared samples were determined from XRD APD2000pro.equipped with $CuK_\alpha$ as a radiation source of wavelength $\lambda = 1.54056$ Aº.

#### 2.3.2.FTIR

The chemical structure and function groups of samples were measured by Fourier Transform Infrared (FTIR) spectroscopy (Thermo Nicolet, FTIR, and NEXUS) in the range from 4000 up to 400 $cm^{-1}$. KBr disc technique is applied in the present work. 1 mg of dried samples mixed with 200 mg of KBr (1%), then grounded to fine powder and pressed under vacuum to a pellet. The disc diameter is equal to that of the instrument's measuring window and is about 1mm thick. The IR absorption spectra were measured immediately after preparing the discs.

#### 2.3.3. Raman spectroscopy

Raman spectra characterization was achieved using the 514.5 nm lines from argon ion laser and examined using a Jobin Yvon T64000 spectrometer equipped with a charge-coupled device. An optical microscope was used to focus the light incident on a spot of about

2 µm in diameter on the sample. Unpolarized Raman spectra were achieved in backscattering geometry.

**2.3.4. Linear transmission measurements**

The transmission was measured in the range between (300 and 900 nm) using JASCO V-570 UV/VIS/NIR spectrophotometer. The instrument is specified by resolution of 0.1 nm and wavelength accuracy ±0.3 nm (at a spectral bandwidth of 0.5 nm). The measurements were made on glass, immediately after glass preparation and all spectra were measured at room temperature.

## 3. Results and Discussions

### 3.1. The XRD patterns of nano-composites ST0.4HM and ST0.4H0.5YM, both annealed at different temperature

Fig.1. (A and B) presents the XRD spectra of the nano-composites ST0.4HM (A) and ST0.4H0.5YM (B), both annealed at different temperatures of 500, 800, and 1000ºC, respectively, for 3h.

Corresponding to the XRD patterns of ST0.4H annealed at different temperatures 500, 800 and 1000ºC, it is clearly seen that the principle peak at 2Θ° = 27.6º corresponds to (110) plane of rutile phase increases in intensity by increasing the temperature from 500 up to. In contrary at 2Θ° = 25.2°, which is attributed to the anatase (101) plane we obtained an opposite trend, while it exhibits a higher intensity at 500ºC. Moreover, the two peaks at 2Θ° = 20.7 and 22.5º are due to the host material silica alpha cristobalite phase. The C.S. of ST0.4HM annealed at 500ºC decreased from 38 to 16 nm than the C.S. of the same sample at 1000ºC. This observation may have resulted from the formation of the Si-O-Ti bond, meaning the strong interaction between titania and silica at low temperature which would prevent the growth of the crystalline size of $TiO_2$ particles, which is in agreement with FTIR results as shown in Fig.2. Moreover, $Ho^{3+}$ ions with (0.9) ionic radii value caused significant changes in the crystalline lattice by substituting the $Ti^{4+}$ with (0.68) ionic radii value. This substitution may cause internal stress in the crystal which is associated with coarse and fine grains in the ceramics, and as result, the size decreases [34]. It is seen from Table 2. that the C.S. of all samples increased by increasing the annealing temperature from 500 up to 1000ºC.

Fig.1. (B) illustrates the effect of increasing the temperature on the XRD patterns of ST0.4H0.5YM nanocomposite oxides. The XRD patterns of the prepared sample for ST0.4H0.5YM were annealed at 500, 800, and 1000ºC for 3 hours, all prepared by sol-gel technique. The results indicated that the main peak at 2Θ° = 27.2, 36.2, and 53.7° corresponds to (110), (101), and (211) respectively planes of the rutile phase which is in agreement with [JCPDS 088-1173] cards. Where it is seen that the principle peak at 2Θ° = 27.2° corresponds to (110) plane of rutile phase increases in intensity by increasing the temperature from 500 up to 1000° C.

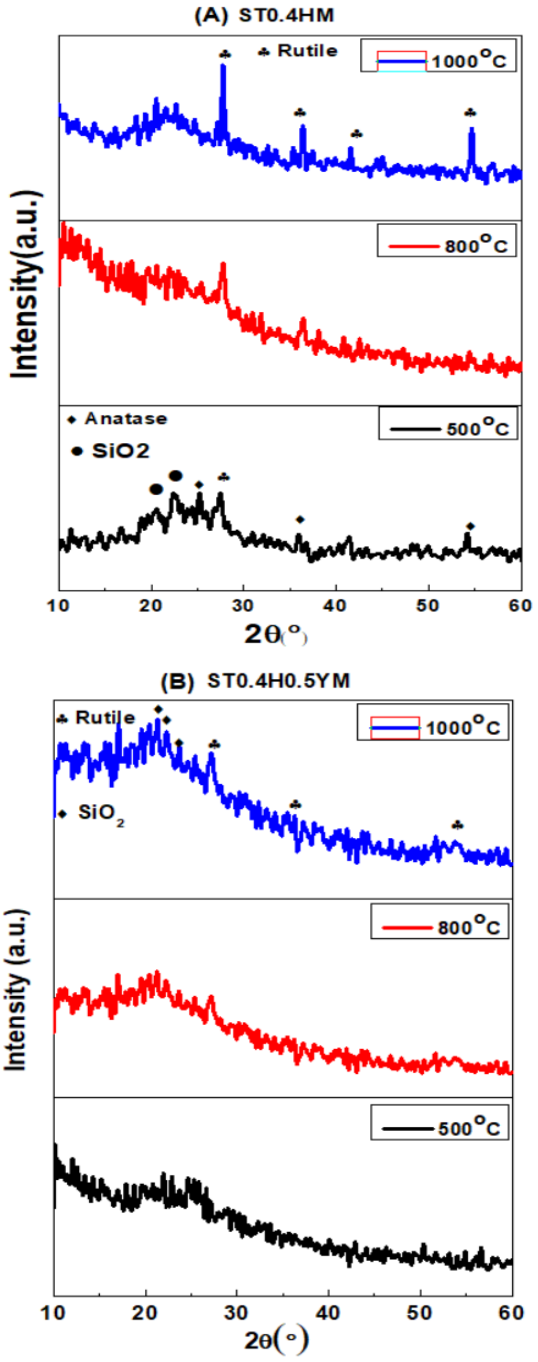


Fig.1. (A &B) The XRD patterns of nano-composites ST0.4HM (A) and ST0.4H0.5YM (B), both annealed at different temperatures of 500, 800, and 1000ºC, respectively, for 3h.

Moreover, increasing the temperature up to1000°C led to the transformation from the amorphous phase of silica to the crystalline α-cristobalite phase of silica with the [JCPDS Card No. 39-1425], appears at 2Θ =20.5, 21.4, 22.3 and 23.3°, which are corresponding to (100), (111), (212), and (113) plans of tetragonal

structure silica. It is detected that in $Ho^{3+}$/$Yb^{3+}$ions Co-doped samples there is no obvious secondary phase appeared, referring to $Ho^{3+}$ and/or$Yb^{3+}$ ions, so these ions are completely embedded in the STM crystal lattice. Moreover, co-doped with $Yb^{3+}$ ions causes significant changes in the crystalline lattice due to the substitution of $Ti^{4+}$ by $Ho^{3+}$ and $Yb^{3+}$ ions, where they have larger ionic radii values than $Ti^{4+}$ as follows: ( $Ti^{4+}$)(0.61 Å), (Ho) (0.9 Å ) and (Yb) (0.87 Å), respectively. It's clearly observed that the crystallite size decreased by increasing $Yb^{3+}$ ions concentration. this may be due to increased stress in the crystal [4]. The crystallite sizes of ST0.4H0.5YM were calculated at both 800 and 1000ºC using Scherrer's equation, we found that the C.S. increased from 11 up to 16 nm, respectively.

For comparison between Fig 1 (A) and (B) it is clearly seen that by doping with Yb ions a decrease in intensity than in the case of doped with $Ho^{3+}$ alone is present. Moreover, the crystallite sizes decrease.

### 3.2. FTIR Spectra of ST0.4HM co-doped with (0.5,0.75 and 1) mol. % $Yb^{3+}$ions.

Fig.2. displays the FTIR spectra of ST0.4H0.5YM, ST0.4H0.75YM, and ST0.4H1YM after annealing at 500º C for 3h. It is observed from the figure that in all samples, a broad absorption band appeared at waves 3308 and 1629 $cm^{-1}$, assigned to the stretching vibration of hydrogen bond O-H. Two bands appeared at 1055 and 942 $cm^{-1}$ assigned to asymmetric Si-O-Si stretching vibrations and Si–O–Ti vibrations, respectively. In addition, a band observed at 792 $cm^{-1}$, this band is due to the asymmetric stretching vibrations of Ti–O bonds of the $TiO_4$ tetrahedral. Another observed absorption band appeared at wavenumber 431 $cm^{-1}$, assigned to Si-O-Si bending vibrations.

Fig.3. and 4. show the FTIR spectra of ST0.4HM co-doped with (0.5, 0.75, and 1) mol % $Yb^{3+}$; (ST0.4H0.5YM, ST0.4H0.75YM, and ST0.4H1YM) annealed at 800 and 1000ºC. By comparing the effect of increasing temperature from 500ºC up to 800 and 1000ºC, it is clear that the bands that appeared at 3308 and 1629$cm^{-1}$ are disappeared due to the high annealing temperature at 800 and 1000ºC. The absorption band at 1055 $cm^{-1}$ shifted to higher wavenumber 1062 and 1074 $cm^{-1}$ by increasing the temperature up to 800 and 1000ºC, respectively. At 800ºC the absorption band appeared at 942 $cm^{-1}$ is shifted to a higher wavenumber 949 $cm^{-1}$ with (0.5, 1mol %) of $Yb^{3+}$ ions and appeared in the same position with 0.75mol % of $Yb^{3+}$ ions. Nearly the same band position appeared in all concentrations of $Yb^{3+}$ ions annealed at 1000ºC. Moreover, the absorption band appeared at 792$cm^{-1}$ shifted to a higher wavenumber 797 $cm^{-1}$ in all concentrations of $Yb^{3+}$ ions annealed at 800 and 1000ºC. Furthermore, a new absorption band was observed at wavenumber 645 $cm^{-1}$ after increasing the temperature to 1000ºC, this can be attributed to the stretching vibration of Ti-O-Ti and Ti-O bonds in the $TiO_2$ crystalline structure. The band appeared at 431 $cm^{-1}$ is shifted to higher wavenumber 447 and 454 $cm^{-1}$ in all concentrations of $Yb^{3+}$ ions annealed at 800 and 1000ºC.On the other hand, it was observed that the intensity of all the absorption bands increases with increasing the annealing temperature up to 1000ºC. The bands are summarized and assigned in Table 2. The molecular signature of the samples was confirmed by FT-IR studies.

Table 2 Comparison between the observed wave numbers ($cm^{-1}$) from FT-IR spectra of ST0.4H0.5YM, ST0.4H0.75YM, and ST0.4H1YM

| Wave number (cm−1) | | | Assignment |
|---|---|---|---|
| at 500°C | at 800°C | at1000°C | |
| 3308, 1629 | -------- | ---------- | stretching vibration of hydrogen bond O-H. |
| 1055 | 1062 | 1074 | asymmetric Si-O-Si stretching vibrations |
| 942 | 949 | 949 | Si–O–Ti vibrations |
| 792 | 797 | 797 | Asymmetric stretching vibrations of Ti–O bonds of the $TiO_4$ tetrahedral |
| ---------- | ---------- | 645 | Ti-O-Ti and Ti-O bonds in the $TiO_2$ crystalline structure |
| 431 | 447 | 454 | Si-O-Si bending vibrations. |

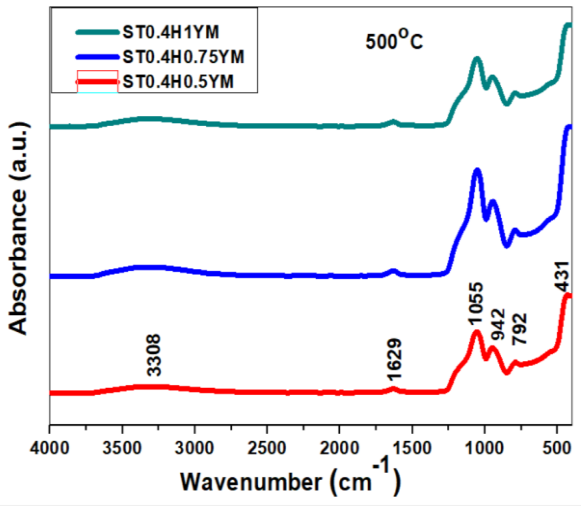


Fig.2. The FTIR spectra of ST0.4H.05YM, ST0.4H0.75YM, andST0.4H1YM, respectively annealed at 500ºC for 3h.

### 3.3. The effect of increasing temperature on the Raman Spectra of ST 0.4HM.

Fig.5. shows the Raman spectra of ST0.4H0.5YM, annealed at different temperatures (500, 800, and 1000°C). For the sample annealed at 500ºC, the band at 475$cm^{-1}$ was present which is attributed to the

anatase phase. Moreover, the two bands at 963 and 1330 $cm^{-1}$ represent the Si-Si stretching and stretching vibrations of Si-OH, respectively. By comparing the spectra of all concentrations of $Yb^{3+}$ ions annealed at 500 with all concentrations of $Yb^{3+}$ ions annealed at 800 and 1000°C, it is clear that the 147 $cm^{-1}$ band is the strongest observed band for the rutile phase at the higher annealing temperature. The band appeared at 475 $cm^{-1}$ and shifted to lower wavenumber 435 and 415 $cm^{-1}$ at 800 and 1000°C, respectively which are assigned to the rutile phase,. The band at 615 $cm^{-1}$appeared clearly after being annealed at 800°C, which is assigned to the anatase phase. The band at 622 $cm^{-1}$ assigned to rutile, appears after annealing at 1000°C.

### 3.4 optical transmission and structural morphology of thin films

Fig.6 a. shows the transmittance (%) for ST0.4H0.5YT, ST0.4H0.75YT, and ST.4H1YT respectively annealed at a constant temperature of 500°C for 3h. Transmittance results revealed higher transmittance in visible range 300 – 900 ranging from about 83 up to more than 94 % informing higher film transparency. It is observed that the ST0.4H0.5YT transmittance is the highest among all the transmittance prepared films equal to (94%), in addition, the transmittance decreases as the $Yb^{3+}$ ions concentration increases up to 1 mol.% due to the increase in the density at the highest $Yb^{3+}$ ions concentration. From these results, it can be concluded that by both doing with 0.4 mol. % of $Ho^{3+}$ ions and co-doped with 0.5 mol. % of $Yb^{3+}$ ions, (ST0.4H0.5YT) sample have enhanced transmittance %.

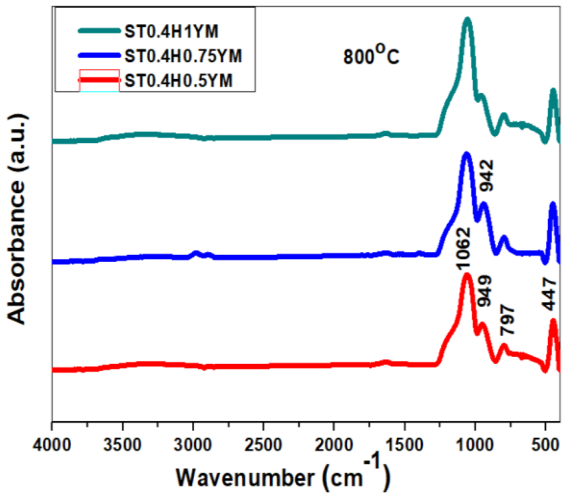


Fig.3. The FTIR spectra of ST0.4H.05YM, ST0.4H0.75YM, and ST0.4H1YM, respectively annealed at 800°C for 3h.

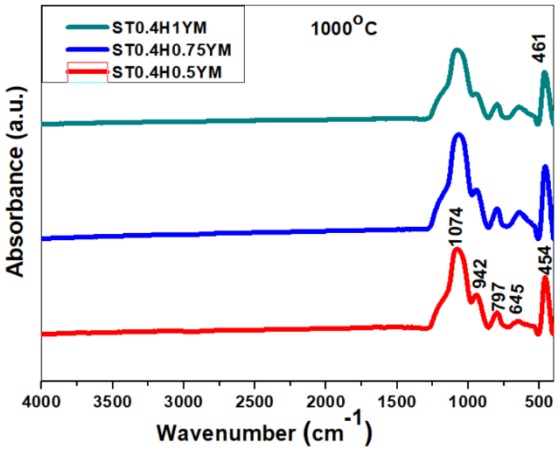


Fig.4. The FTIR spectra of ST0.4H.05YM, ST0.4H0.75YM, and ST0.4H1YM, respectively annealed at 1000°C for 3h.

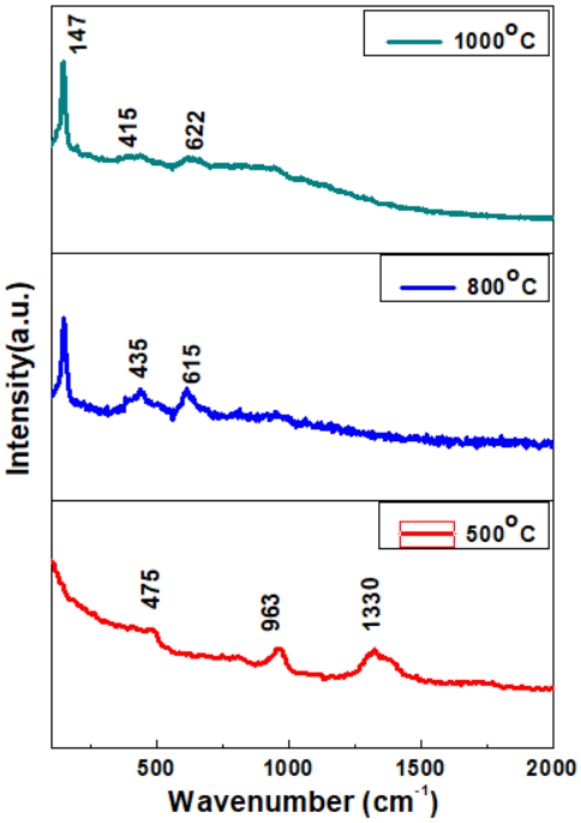


Fig.5. The Raman spectra of ST0.4H0.5YM, annealed at different temperatures (500, 800 and 1000°C).

### 3.5. Field Emission Scanning Electron Microscope (FESEM) characterization

To study the effect of increasing the annealing temperature from 500 up to 1000°C on the surface morphology nature and cross sections of ST0.4H0.5YT nano-composite and on the thickness of the mentioned films shown in Fig. 7 (a-d), were drawn.

Fig. 7 (a & c) show the FESEM surface morphology of the ST0.4H0.5YT nano-composite thin film however, the Fig. 7. (b & d) show the cross sections view, respectively. The surface of the film annealed at 500ºC exhibits a rigid nature not homogeneous with some bloats inside it due to residual water content at this considerably low temperature. Moreover, the surface is not so compact, Fig. 7 (a). While by heating the sample at 1000ºC the same film shows homogeneity, good uniformity, smooth and dense surface with cracks free almost adhere well to the substrate, Fig 6 (c).ó While, Fig.7 (b, & d), illustrates the FESEM cross sections view of the of ST0.4H.05YM, annealed at higher temperature 1000ºC, for 3h. By increasing the temperature the thickness will be decreased. From the figures it is clearly appeared that it exhibited higher thickness with average value equal about ~2.9 µm, (b) at lower temperature 500ºC. Generally, by increasing the preparation temperature of the nano-composite samples results in lower thickness values giving the following mean obtained data for (d) at 1000ºC ~ 1.28175 µm.

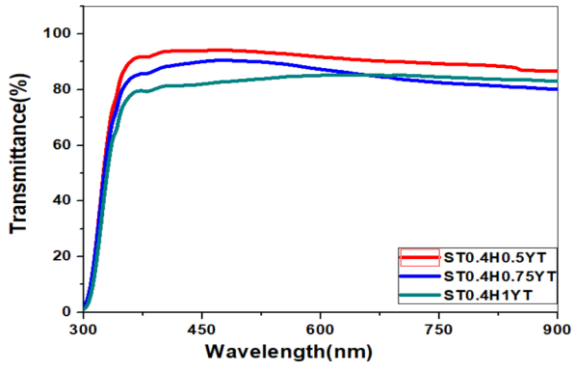


Fig.6. Transmittance (%) for ST0.4H0.5YT, ST0.4H0.75YT, and ST0.4H1YT, respectively annealed at 500ºC for 3h. (b) The FESEM cross section view of the ST0.4H0.5YT

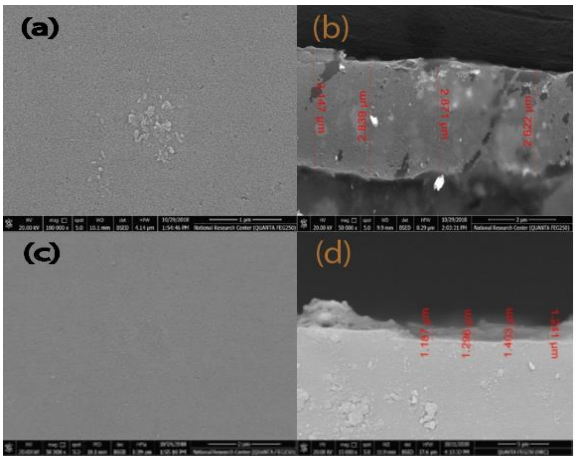


Fig.7. (a - d) The FESEM micrographs and cross sections view of ST0.4H.05YM, annealed at (a & b) 500ºC, (c & d) 1000ºC, respectively for 3h.

## *Conclusions*

the preparations of $Ho^{3+}$: $Yb^{3+}$ ions doped $SiO_2$- $TiO_2$ nano-composite were carried out via a modified sol–gel method at different annealing temperature ranging from 500ºC up to 1000ºC for 3h. XRD spectra reveals that samples annealed 500,800 and 1000ºC are formed in nano-composite tetragonal shape. It is well seen that the C. S. of all prepared samples increased by increasing the annealing temperature from 500 up to 1000ºC, giving the following values; 38 to 16 nm at 500 and 1000ºC, while for ST0.4H0.5YM equal to 11 up to 16 nm from 500ºC up to 1000ºC, respectively. FTIR spectra confirm the strong interaction between titania and silica via the 942$cm^{-1}$ band which is assigned to Si–O–Ti vibration mode. Raman spectra show anatase and rutile spectral features in the sample annealed up to 800ºC. The change from anatase to rutile transition of the monolith samples was detected at 1000ºC. The thickness of the thin film was measured using FESEM which reveals that the thickness possesses exhibit ~ 1.28175 µm at 1000ºC, while it increases at lower temperature 500ºC to be equal to ~2.9 µm. The UV –Visible also confirmed high transparency for the prepared films annealed at 500ºC. It can be seen that the highest among all the transmittance is observed at 0.4 mol. % $Ho^{3+}$ ions co-doped with 0.5mol.% $Yb^{3+}$, it is greater than 94 %.

## References

[1] I. K. Ahmed, E. H., Amin, A., Ayoub, M. M. H., Hashem, A. I., & Battisha, "Physical Properties of Tb3+ and Ho 3+ Ions Embedded in Nanocomposites Phospho-Silicate.," *Acta Phys. Pol. A*, vol. 137, no. 6, pp. 1037–1042, 2020.

[ 2] A. Amin *et al.*, "Phosphosilicate–polyamidoamine hyperbranched polymer–Er 3+ nanocomposite toward planar optical waveguide applications," *Polym. Compos.*, vol. 40, no. 5, pp. 2029–2038, May 2019, doi: 10.1002/pc.24984.

[3] A. Salah, S. K. El-Mahy, O. El-sayed, and I. K. Battisha, "Up-conversion behaviors of nano-structure BaTi0.9Sn0.1O3 activated by Er3+/Yb3+ ions," *Optik (Stuttg).*, vol. 209, no. January, p. 164571, 2020, doi: 10.1016/j.ijleo.2020.164571.

[4] Ahmed, E. H., Ayoub, M. M. H., Hashem, A. I., Wickleder, C., Adlung, M., Amin, A., & Battisha, I. K. (2021). Effect of Increasing Temperature on 1.5 µm Spectroscopic Emission of Er 3 Ions Activated Phospho-silicate Thin Film. *International Journal of Photochemistry and Photobiology*, *5*(2), 28.

[5] T. A. Hameed, F. Mohamed, A. M. Mansour, and I. K. Battisha, "Synthesis of Sm 3+ and Gd 3+ Ions Embedded in Nano-Structure Barium

Titanate Prepared by Sol-Gel Technique: Terahertz, Dielectric and Up-Conversion Study," *ECS J. Solid State Sci. Technol.*, vol. 9, no. 12, p. 123005, Dec. 2020, doi: 10.1149/2162-8777/abc96b.

[6] H. Shaier, A. Salah, W. M. Mousa, S. S. Hamed, and I. K. Battisha, "Physical properties and up-conversion development of Ho3+ions loaded in nano-composite silica titania thin film," *Mater. Res. Express*, vol. 7, no. 9, p. 096403, Sep. 2020, doi: 10.1088/2053-1591/abb4fe.

[7] Feenstra, J., Six, I. F., Asselbergs, M. A. H., Van Leest, R. H., de Wild, J., Meijerink, A., ... & Schermer, J. J. (2015). Er 3+/Yb 3+ upconverters for InGaP solar cells under concentrated broadband illumination. *Physical Chemistry Chemical Physics*, *17*(17), 11234-11243.

[8] A. B. Shishmakov, Y. V Mikushina, O. V Koryakova, M. S. Valova, N. A. Zhuravlev, and L. A. Petrov, "Binary ZrO2-SiO2 xerogels: Synthesis and properties," *Russ. J. Inorg. Chem.*, vol. 57, no. 1, pp. 24–27, Jan. 2012, doi: 10.1134/S003602361201024X.

[9] S. Vives and C. Meunier, "Influence of the synthesis route on sol–gel SiO2–TiO2 (1:1) xerogels and powders," *Ceram. Int.*, vol. 34, no. 1, pp. 37–44, Jan. 2008, doi: 10.1016/j.ceramint.2006.08.001.

[10] Y. V Mikushina et al., "TiO2-SiO2 binary xerogels: Synthesis and characterization," Russ. J. Inorg. Chem., vol. 53, no. 10, pp. 1557–1560, Oct. 2008, doi: 10.1134/S0036023608100069.

[11] J. Ren, Z. Li, S. Liu, Y. Xing, and K. Xie, "Silica–Titania mixed Oxides: Si–O–Ti Connectivity, Coordination of Titanium, and Surface Acidic Properties," Catal. Letters, vol. 124, no. 3–4, pp. 185–194, Aug. 2008, doi: 10.1007/s10562-008-9500-y.

[12] M. Schraml-Marth, K. L. Walther, A. Wokaun, B. E. Handy, and A. Baiker, "Porous silica gels and TiO2/SiO2 mixed oxides prepared via the sol-gel process: characterization by spectroscopic techniques," J. Non. Cryst. Solids, vol. 143, pp. 93–111, Jan. 1992, doi: 10.1016/S0022-3093(05)80557-5.

[13] J. L. Lakshmi, N. J. Ihasz, and J. M. Miller, "Synthesis, characterization and ethanol partial oxidation studies of V2O5 catalysts supported on TiO2–SiO2 and TiO2–ZrO2 sol–gel mixed oxides," J. Mol. Catal. A Chem., vol. 165, no. 1–2, pp. 199–209, Jan. 2001, doi: 10.1016/S1381-1169(00)00415-5.

[14] Y. D. Hou et al., "N-Doped SiO2/TiO2 mesoporous nanoparticles with enhanced photocatalytic activity under visible-light irradiation," Chemosphere, vol. 72, no. 3, pp. 414–421, Jun. 2008, doi: 10.1016/j.chemosphere.2008.02.035.

[15] N. Hüsing, B. Launay, D. Doshi, and G. Kickelbick, "Mesostructured Silica−Titania Mixed Oxide Thin Films," Chem. Mater., vol. 14, no. 6, pp. 2429–2432, Jun. 2002, doi: 10.1021/cm011310z.

[16] H. X. Zhang, Y. Zhou, C. H. Kam, Y. L. Lam, and Y. C. Chan, "Preparation and Luminescence of Europium Doped Zinc Silicate Phosphor," MRS Proc., vol. 560, p. 9, Feb. 1999, doi: 10.1557/PROC-560-9.

[17] M. Cason, D. Bersani, G. Antonioli, P. Paolo Lottici, A. Montenero, and M. Cavalli, "Thermal nonlinear refraction in the dye-doped sol–gel xTiO2·(100−x)SiO2 system," Opt. Mater. (Amst)., vol. 12, no. 4, pp. 447–452, Sep. 1999, doi: 10.1016/S0925-3467(98)00073-1.

[18] E. H. Ahmed et al., "Nanocomposites dendritic polyamidoamine-based chitosan hyperbranched polymer embedded in silica – phosphate for waveguide applications," Polym. Technol. Mater., vol. 60, no. 7, pp. 744–755, May 2021, doi: 10.1080/25740881.2020.1844235.

[19] Shaker, Z., El-shaarawy, M., Shash, N., Khoder, H., Battisha, I., & Salem, M. A. (2021). Nano-composite Phospho-silicate co-doped with Ho3+ and Yb3+ ions for new up-down-shifting applications. Egyptian *Journal of Chemistry*, *64*(12), 2-3., doi: 10.21608/ejchem.2021.78927.3861.

[20] D. Atta, M.M. Ismail, I.K. Battisha, (2022), 3D laser Raman micro-spectroscopy of $Er^{3+}$ and $Yb^{3+}$ co-activated nano-composite phosphosilicate for industrial photonics applications, Optics and Laser Technology, 149, 107761, https://doi.org/10.1016/j.optlastec.2021.107761

[21] A. Elbanna, D. Atta, D. Sherief, (2022), In vitro bioactivity of newly introduced dual-cured resin-modified calcium silicate cement, Dental Research Journal, 19, 1, https://doi.org/10.4103/1735-3327.336686

[22] A. Refaat, D. Atta, O. Osman, A.A. Mahmoud, S. El-Kohadary, W. Malek, M. Ferretti, H. Elhaes, H., M. Ibrahim,(2019), Analytical and computational study of three coptic icons in saint mercurius monastery, Egypt, Biointerface Research in Applied Chemistry, 9, 4685–4698, https://doi.org/10.33263/BRIAC96.685698.

[23] N.M.Farrage, A.H. Oraby, E.M.M. Abdelrazek, D. Atta,(2019), Synthesis, characterization of Ag@PANI core-shell nanostructures using solid state polymerization method, Biointerface Research in Applied Chemistry, 9, 3934–3941, https://doi.org/10.33263/BRIAC93.934941.

[24]

D.Atta, A. Fakhry, M. Ibrahim,(2015), Chitosan membrane as an oil carrier: Spectroscopic and modeling analyses, Der Pharma Chemica,7,357–361.

[25] D. Atta, A. Okasha, M. Ibrahim,(2016), Setting up and calibration of simultaneous dual color wide field microscope for single molecule imaging, Der Pharma Chemica, 8,76–82.
[26] D. Atta, A. Okasha, (2015),Single molecule laser spectroscopy, Spectrochimica Acta, 135,1173-1175. https://doi.org/10.1016/j.saa.2014.07.085
[27] Mahmoud M.Ismail, Inas K.Batisha,Lidia Zur, Alessandro Chiasera, MaurizioFerrari, AnnaLukowiak, Optical properties of $Nd^{3+}$-doped phosphate glasses, Optical materials J., Opt. Mater., 99, (2020) 109591, http://www.elsevier.com/locate/optmat.
[28] Talaat A. Hameed, F. Mohamed, A. M. Mansour, I. K. Battisha, Synthesis of $Sm^{3+}$ and $Gd^{3+}$ ions embedded in nano-structure Barium Titanateprepared by sol gel technique: Terahertz, Dielectric and Up conversion study, J. of ECS Journal of Solid State Science and Technology, ECS J SOLID STATE SC, published, November, 9 123005, (2020).
[29] O. Osman, A. Mahmoud, D. Atta, A. Okasha, M. Ibrahim,(2015), Computational notes on the effect of solvation on the electronic properties of glycine, Der Pharma Chemica, 7, 377–380.
[30] N.M.Farrage, A.H. Oraby, E.M.M. Abdelrazek, D. Atta,(2019), Molecular Electrostatic Potential Mapping for PANI Emeraldine Salts and Ag@PANI core-shell, Egyptian Journal of Chemistry, 62, 99–109, https://doi.org/10.33263/BRIAC93.934941.
[31] A. Sarhan1, A.M. Abdelghany, F. El- Dossoki, (2022), Synthesis and characterization of nano CuO/ZnO/Al2O3 catalyst via Laser ablation route for the preparation of some cyanoacetanilide derivatives, Egyptian Journal of Chemistry, 65, 275-279,https://doi.org/10.21608/EJCHEM.2021.103671.4798.
[32].Okasha, D. Atta, W.M. Badawy, M. V. Frontasyeva, H. Elhaes, M. Ibrahim, (2017), Modeling the coordination between Na, Mg, Ca, Fe, Ni, and Zn with organic acids, Journal of Computational and Theoretical Nanoscience, 14, 1357–1361, 8j